様　式　Ｃ－１９、Ｆ－１９－１、Ｚ－１９　（共通）

科学研究費助成事業　　研究成果報告書

平成　２９　年　　６　月　　７　日現在

機関番号：８２１０８
研究種目：基盤研究(C)（一般）
研究期間：2014～2016
課題番号：２６４００３２３

研究課題名（和文）Electron and phonon transport in single crystal tetragonal niobium bronzes

研究課題名（英文）Electron and phonon transport in single crystal tetragonal niobium bronzes

研究代表者
ＫＯＬＯＤＩＡＺＨＮ　Ｔａｒａｓ（Kolodiazhnyi, Taras）

国立研究開発法人物質・材料研究機構・機能性材料研究拠点　強相関物質グループ・主幹研究員

研究者番号：８０４６９７６７

交付決定額（研究期間全体）：（直接経費）　　3,300,000円

研究成果の概要（和文）：タングステンブロンズBa6-xSrxNb10030においてBaとSrが全率固溶することが分かった。2-400Kにおいて熱伝導率の温度変化を測定したところSr置換により熱伝導率が大幅に減少するとともに、x>3において30K付近で温度依存性がほとんどなくなるという振る舞いを見いだした。これは本来ガラスで生じるような振る舞いである。
我々はこの振る舞いの原因を、イオン半径の違いにより原子変位パラメータに異常が生じるものとして説明した。また、固溶系の電気抵抗測定により、Sr量を変えると異常金属から絶縁体へ転移することが分かった。さらにBa濃度が高い場合にはTc～1.6Kの超伝導が発現することを発見した。

研究成果の概要（英文）：Solid solution of Ba6-xSrxNb10030 crystalizes in filled tetragonal tungsten bronze (TTB) structure. Our results indicate that the Ba and Sr ions show complete solid solution without miscibility gap. We studied the x dependence of thermal conductivity of polycrystalline Ba6-xSrxNb10030 samples measured in the 2-400 K temperature interval. Substitution of Sr for Ba brings about a significant decrease in thermal conductivity at x>3 accompanied by development of a low-temperature (T = 10-30 K) plateau region reminiscent of a glass-like compounds. We explain this behavior based on a size-driven site occupancy and atomic displacement parameters. Measurement of the electron transport of the Ba6-xSrxNb10030 solid solution reveals an unusual metal to insulator transition which occurs upon contraction of the unit cell. Another important finding of this project was the discovery of the low-temperature superconductivity at Tc<1.6 K in the Ba-rich members of the Ba6-xSrxNb10030 solid solution.

研究分野：Functional ceramics

キーワード：tetragonal bronze　thermal conductivity　thermoelectric power　charge density wave　anderson localization

１．研究開始当初の背景

In order to successfully compete on a large scale with other technologies for waste heat energy recovery, future thermoelectric materials and devises must have a very high 'thermoelectric figure of merit', $zT > 2$, and also be non-toxic and cheap. These are extremely challenging requirements given that the best industrial-scale thermoelectrics with $zT \leq 1.5$ are based on highly-toxic, chalcogenide binary compounds e.g., Pb-Te-Se-Tl, or prohibitively expensive Ga-Yb-Mn-Sb Zintl phase alloys. It is obvious that to satisfy the above technical and environmental requirements, novel thermoelectric materials with superior performance must be discovered.

２．研究の目的

It is known that many good thermoelectric materials, PbTe being one of them, are found very close to the ferroelectric type lattice instability. Therefore, the goal of this project was to explore the relaxor-type ferroelectric Nb-based tetragonal bronzes from the point of view of their potential applications in high-performance, non-toxic and industrially-scalable bulk thermoelectric devices. The main idea of the project is based upon a concept of 'ferroelectric (FE) thermoelectrics' which exploits non-centrosymmetric metals and semiconductors with high Seebeck coefficient, S, low thermal conductivity, κ, and high charge-carrier conductivity, σ, to maximize the zT value, where $zT = TS^2\,\sigma / \kappa$. A starting point of the project was a relaxor FE $Ba_{1-x}Sr_xNb_2O_6$ insulator (Fig. 1). Because of significant cation disorder on the Ba/Sr-sublattice, this material has rather low thermal conductivity (κ = 2 $Wm^{-1}K^{-1}$ at 400 K) that shows glass-like temperature dependence both along the *a*- and *c*-axis. At the same time, undistorted corner-sharing NbO_6 octahedra that form quasi-1-dimensional (Q1D) chains along the *c*-axis (see Fig. 1) offer an excellent path for high-conductivity charge transport.

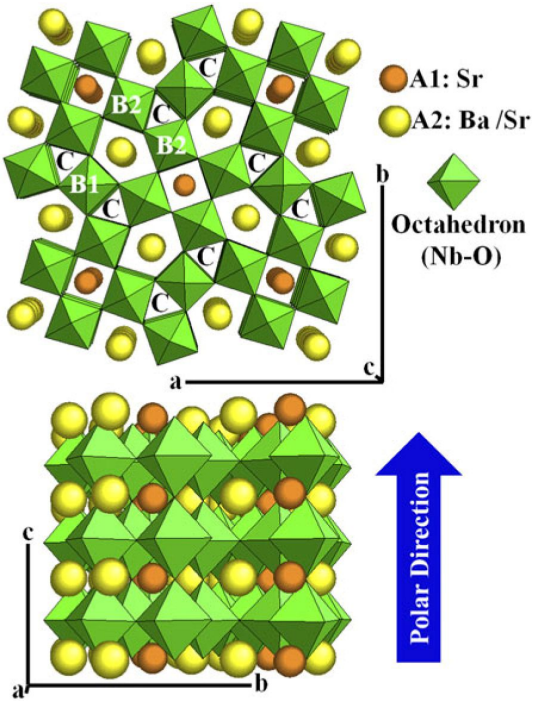

Figure 1. Crystal structure for $(Sr,Ba)Nb_2O_6$ showing connectivity of NbO_6 octahedra.

３．研究の方法

A series of the single crystals and ceramics along the $Ba_{1-x}Sr_xNb_2O_6$–$(Ba_{1-x}Sr_x)_3Nb_5O_{15}$ tie line were prepared using the growth from the melt and solid-phase sintering. Their physical properties including crystal structure, electron and thermal conductivity, specific heat, Seebeck coefficient, electron mobility and magnetic susceptibility were analyzed.

４．研究成果

Solid solution of $Ba_{6-x}Sr_xNb_{10}O_{30}$ crystalizes in filled tetragonal tungsten bronze (TTB) structure described by a general formula $A1_2A2_4B1_2B2_8C_4O_{30}$. Our results indicate that the Ba and Sr ions show complete solid solution without miscibility gap. Some preferential occupancy of the A1 site with Sr and A2 site with Ba ion has been detected. Our most recent results indicate that the Sr end member show lower crystal symmetry than the rest of the $Ba_{6-x}Sr_xNb_{10}O_{30}$ compounds. The Ba-end member crystallizes in the highest symmetry P4/mbm space group ($a = b$ = 1.25842(18) nm and c = 0.39995(8) nm) and so do all the compositions with $0 < x < 5$. We were able to prepare $Sr_6Nb_{10}O_{30}$ end member single crystal from the melt. The crystal structure analysis of the single crystal indicated that it crystalize in the A*mam* space group with distorted TTB structure. We attribute these distortions to the small size of the Sr ion located in the pentagonal TTB channels. In particular, the A*mam* structure (a^* = 1.7506(4) nm, b^* = 3.4932(7) nm, and c^* = 0.77777(2) nm). The latter space group is related to the parent P4/*mbm* TTB structure as $a^* = 2^{1/2}a$, $b^* = 2*2^{1/2}\,a$, $c^* = 2*c$) shows doubling of the unit cell along the c direction as well as distortions in the *ab* plane which lead to an increase in the *a* and *b* unit cell parameters.

We studied the x dependence of thermal conductivity of polycrystalline $Ba_{6-x}Sr_xNb_{10}O_{30}$ samples measured in the 2 - 400 K temperature interval. Substitution of Sr for Ba brings about a significant decrease in thermal conductivity at x > 3 accompanied by development of a low-temperature (T = 10–30 K) 'plateau' region

reminiscent of a glass-like compounds. We explain this behavior based on a size-driven site occupancy and atomic displacement parameters associated with an alkaline earth atomic positions in the title compounds (Fig. 2).

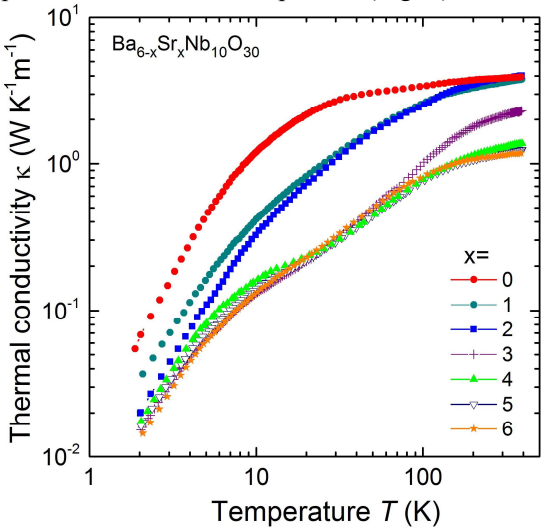

Fig. 2. Thermal conductivity for $Ba_{6-x}Sr_xNb_{10}O_{30}$.

Measurement of the electron transport of the $Ba_{6-x}Sr_xNb_{10}O_{30}$ solid solution reveals an unusual metal to insulator (MIT) transition which occurs upon contraction of the unit cell (Fig. 3). While the Ba-rich compounds are metallic the Sr-rich compounds show an insulating ground state. It is noteworthy that the MIT occurs at $x = 3$, where the glass-like low-temperature thermal conductivity starts to appear.

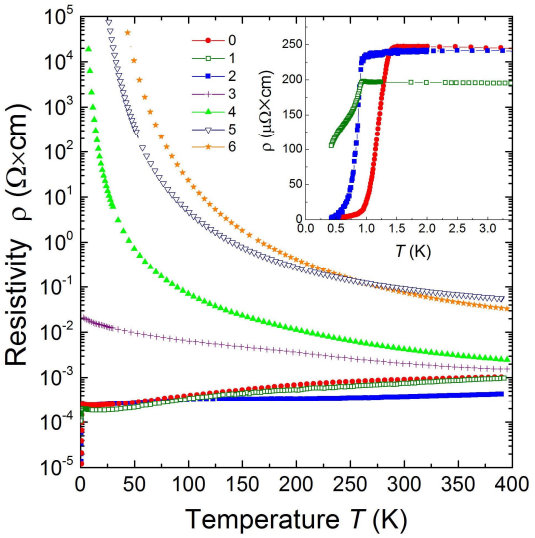

Fig. 3. Electrical resistivity for $Ba_{6-x}Sr_xNb_{10}O_{30}$.

While trying to explain this unusual MIT in $Ba_{6-x}Sr_xNb_{10}O_{30}$ solid solution we considered several possible scenarios including symmetry-driven Mott transition, MIT driven by critical electron concentration, and finally, MIT driven by disorder/random field Anderson localization. Based on the analysis of the experimental data supplemented by calculations of critical electron concentration, we come to conclusions that Anderson localization due to random electric fields is the main driving force for MIT in $Ba_{6-x}Sr_xNb_{10}O_{30}$ solid solution.

Another important finding of this project was the discovery of the low-temperature superconductivity at Tc < 1.6 K in the Ba-rich members of the $Ba_{6-x}Sr_xNb_{10}O_{30}$ solid solution. Analysis of specific heat of the superconducting phase transition points to the conventional s-wave superconductivity in the title compounds with no evidence of the nodal lines or nodal points.

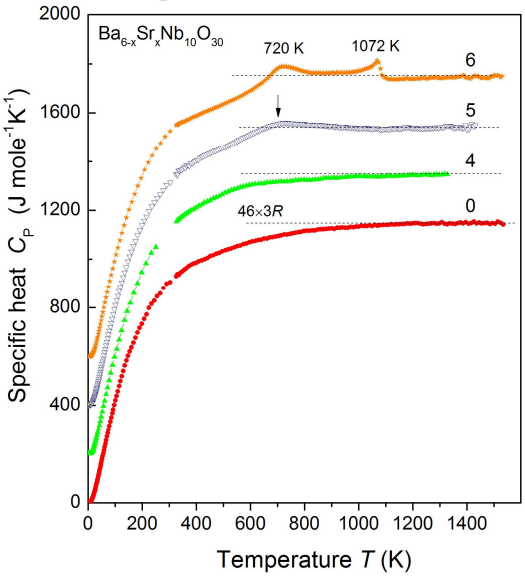

Fig. 4. Specific heat of $Ba_{6-x}Sr_xNb_{10}O_{30}$.

$Ba_{6-x}Sr_xNb_{10}O_{30}$ samples measured in a wide temperature range up to 1500 K. The samples with $x \leq 4$ show no detectable anomalies in the high-T specific heat data. We bring attention to the two high-temperature phase transitions in the $Sr_6Nb_{10}O_{30}$. The first phase transition with a very broad maximum at T ≈ 720 K is somewhat similar to that observed in the non-centrosymmetric $Ba_{1-x}Sr_xNb_2O_6$ unfilled TTBs. At $T \approx 1072$ K another sharp phase transition with a first-order signature is detected (Fig. 4). The later phase transition is very similar to that found by one of us in the $SrTa_2O_6$ and $EuTa_2O_6$ TTBs (not shown here) and is most likely attributed to the doubling of the TTB unit cell along the c-axis. A very broad and weak anomaly in the specific heat of the $BaSr_5Nb_{10}O_{30}$ sample is indicated by a vertical arrow at T ≈ 702 K in Fig.4. It may be associated with a very small structural change in the $BaSr_5Nb_{10}O_{30}$ compound.

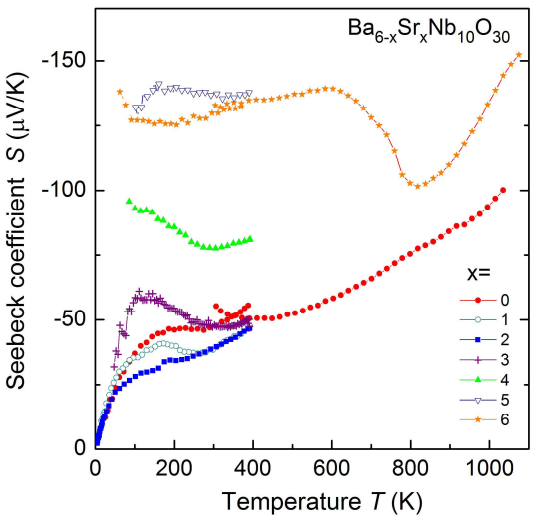

Fig. 5. Temperature dependence of Seebeck coefficient of $Ba_{6-x}Sr_xNb_{10}O_{30}$.

Temperature evolution of the Seebeck coefficient, S, of the $Ba_{6-x}Sr_xNb_{10}O_{30}$ is shown in Fig. 5. As expected, the $Ba_{6-x}Sr_xNb_{10}O_{30}$ with $x \leq 3$ shows metal-like behavior with S increasing gradually with temperature. The samples with insulating ground state (i.e., $x \geq 4$) show much higher S with a somewhat more complex temperature dependence. To better understand this behavior we have expanded the thermopower measurement range for the end members to $T = 1100$ K. Somewhat poor match between the low- and high-T data in the 350-400 K interval is explained by the use of two different experimental setups below and above 400 K. The Seebeck coefficient of the $Ba_6Nb_{10}O_{30}$ end member continues to gradually increase, as expected for metals. The S of $Sr_6Nb_{10}O_{30}$, on the other hand, shows a pronounced anomaly with a strong dip at T ≈ 800 K followed by a steady increase at higher temperatures characteristic of a metal (Fig. 5). It is noteworthy that the steepest drop in the Seebeck coefficient in the $Sr_6Nb_{10}O_{30}$ sample at T ≈ 750 K correlates reasonably well with the broad phase transition at T ≈ 720 K as detected by specific heat measurements. We speculate, therefore, that the transition from the insulating to metallic-type behavior in $Sr_6Nb_{10}O_{30}$ may be associated with the structural phase transition at 720 K.

Also, in parallel development, a tetragonal tungsten bronze polymorph of $EuTa_2O_6$ was prepared and analyzed. $EuTa_2O_6$ crystallizes in the centrosymmetric Pnam space group (with unit cell: $a = 1.23693$ nm, $b = 1.24254$ nm, and $c = 0.77228$ nm) isomorphous with orthorhombic β-$SrTa_2O_6$. Dielectric constant shows a broad peak at ca. 50 K with dielectric dispersion resembling diffuse phase transition. A thermal conductivity of $EuTa_2O_6$ shows a low-temperature ($T \approx 30$ K) "plateau" region reminiscent of a glass-like behaviour in $Ba_{6-x}Sr_xNb_{10}O_{30}$ TTB compounds. This behavior can be attributed to the loosely bound Eu^{2+} ions occupying large tricapped trigonal prismatic sites in the $EuTa_2O_6$ structure.

5．主な発表論文等
（研究代表者、研究分担者及び連携研究者には下線）

〔雑誌論文〕（計 12 件）

① T. Kolodiazhnyi, T. Charoonsuk, Y.-S. Seo, S. Chang, N. Vittayakorn, J. Hwang, Magnetic, optical and electron transport properties of n-type CeO_2: Small polarons versus Anderson localization. *Phys. Rev. B* 査読有 **95**, 045203 (2017).

② T. Charoonsuk, N. Vittayakorn, T. Kolodiazhnyi, Defect chemistry of Ta-doped CeO_2. *J. Alloys Comp.* 査読有 **695**, 1317-1323 (2017).

③ I. V. Solovyev, T. Kolodiazhnyi, Origin of magnetoelectric effect in $Co_4Nb_2O_9$ and $Co_4Ta_2O_9$: The lessons learned from the comparison of first-principles-based theoretical models and experimental data. *Phys. Rev. B*, 査読有 **94**, 094427 (2016).

④ T. Kolodiazhnyi, H. Sakurai, A. A. Belik, O. V. Gornostaeva. Unusual lattice evolution and magnetochemistry of Nb doped CeO_2. *Acta Materialia* 査読有 **113**, 116-123 (2016).

⑤ S. Forbes, F. Yuan, K. Kosuda, T. Kolodiazhnyi, Y. Mozharivskyj. Investigation of the transport properties and compositions of the $Ca_2RE_7Pn_5O_5$ series (RE is a rare-earth metal, Pn = Sb, Bi), *J.Solid State Chem.* 査読有 **242**, 148-154 (2016).

⑥ S. Forbes, F. Yuan, K. Kosuda, T. Kolodiazhnyi, Y. Mozharivskyj. Synthesis, crystal structure, and physical properties of the Gd_3BiO_3 and $Gd_8Bi_3O_8$ phases. *J. Solid State Chem.* 査読有 **233**, 252-258 (2016)

⑦ T. Kolodiazhnyi, H. Sakurai, M. Isobe, Y. Matsushita, S. Forbes, Y. Mozharivskyj, T. J. S. Munsie, G. M. Luke, M. Gurak, D. R. Clarke. Superconductivity and crystal structural origins of the metal-insulator transition in

$Ba_{6-x}Sr_xNb_{10}O_{30}$ tetragonal tungsten bronzes. *Phys. Rev. B* 査読有 **92**, 214508 (2015).
⑧ T. Kolodiazhnyi, H. Sakurai, O. Vasylkiv, H. Borodianska, Y. Mozharivskyj. Abnormal thermal conductivity in tetragonal tungsten bronze-type $Ba_{6-x}Sr_xNb_{10}O_{30}$. *Appl. Phys. Lett.* 査読有 **104**, 111903(2014).
⑨ T. Kolodiazhnyi, H. Sakurai, O. Vasylkiv, H. Borodianska, S. Forbes, Y. Mozharivskyj. Structure and physical properties of $EuTa_2O_6$ tungsten bronze polymorph. *Appl. Phys. Lett.* 査読有 **105**, 062902(2014).
⑩ T. Kolodiazhnyi, H. Sakurai, Y. Matsushita, Structure, magnetism, specific heat, and dielectric properties of $Eu_2Ta_2O_7$. *Appl. Phys. Lett.* 査読有 **105**, 202903 (2014).
⑪ T. Kolodiazhnyi, Origin of extrinsic dielectric loss in 1:2 ordered, single-phase $BaMg_{1/3}Ta_{2/3}O_3$. *J. Eur. Ceram. Soc.* 査読有 **34**, 1741-1753 (2014).
⑫ B. J. Kennedy, G. Murphy, E. Reynolds, M. Avdeev, H. R. Brand, T. Kolodiazhnyi, Studies of the antiferrodistortive transition in $EuTiO_3$. *J. Phys. Cond. Matter.* 査読有 **26**, 495901 (2014).

〔学会発表〕(計 1 件)

T. Kolodiazhnyi, Effect of local lattice disorder on the metal insulator transition in $Ba_{6-x}Sr_xNb_{10}O_{30}$ tetragonal niobium bronzes. The 7 th International Conference on Electroceramics (ICE2015). State College, Penn State University, Pennsylvania, U.S.A. May 13 -- 16, 2015.

〔図書〕(計 0 件)

〔産業財産権〕

○出願状況(計 0 件)

名称：
発明者：
権利者：
種類：
番号：
出願年月日：
国内外の別：

○取得状況(計 0 件)

名称：
発明者：
権利者：
種類：
番号：
取得年月日：
国内外の別：

〔その他〕
ホームページ等

６．研究組織
(1)研究代表者
KOLODIAZHNYI TARAS
物質・材料研究機構・機能性材料研究拠点
強相関物質グループ・主幹研究員
研究者番号：*80469767*

(2)研究分担者
( )

研究者番号：

(3)連携研究者
( )

研究者番号：

(4)研究協力者
( )